CHALMERS
UNIVERSITY OF TECHNOLOGY

Localization Error Bounds for 5G mmWave Systems under I/Q Imbalance

Citation for the original published paper (version of record):
Ghaseminajm, F., Abu-Shaban, Z., Ikki, S. et al (2020). Localization Error Bounds for 5G mmWave Systems under I/Q Imbalance. IEEE Transactions on Vehicular Technology, 69(7): 7971-7975. http://dx.doi.org/10.1109/TVT.2020.2991377

Localization Error Bounds For 5G mmWave Systems Under I/Q Imbalance

Fariba Ghaseminajm, Zohair Abu-Shaban *Senior Member, IEEE*, Salama S. Ikki *Senior Member, IEEE*, Henk Wymeersch *Senior Member, IEEE*, and Craig R. Benson *Member, IEEE*.

***Abstract*—Location awareness is expected to play a significant role in 5G millimeter-wave (mmWave) communication systems. One of the basic elements of these systems is quadrature amplitude modulation (QAM), which has in-phase and quadrature (I/Q) modulators. It is not uncommon for transceiver hardware to exhibit an imbalance in the I/Q components, causing degradation in data rate and signal quality. Under an amplitude and phase imbalance model at both the transmitter and receiver, 2D positioning performance in 5G mmWave systems is considered. Towards that, we derive the position and orientation error bounds and study the effects of the I/Q imbalance parameters on the derived bounds. The numerical results reveal that I/Q imbalance impacts the performance similarly, whether it occurs at the transmitter or the receiver, and can cause a degradation up to 12% in position and orientation estimation accuracy.**

I. Introduction

Millimeter-wave (mmWave) systems is a major topic contributing to enhancing the fifth generation (5G) mobile communication systems. They offer high bandwidth, leading to higher data rates, and use carrier frequencies from 30 GHz to 300 GHz [1]. In parallel, location-aided systems in 5G are numerous and serve in a wide range of applications such as vehicular communications and beamforming.

Due to the employment of antenna arrays at both the base station (BS) and user equipment (UE), single-anchor localization through the estimation of the directions of arrival and departure (DOA, DOD) and the time of arrival (TOA) is possible. Single-anchor localization bounds for 5G mmWave systems have been widely considered in the literature. For example, in [2], the 3D position error (PEB) and the orientation error bounds (OEB) have been studied for uplink and downlink localization, while [3] proposed position and orientation estimators for 2D positioning. In [4], the authors investigated the probability of 5G localization with non-line-of-sight paths, while [5] investigated localization bounds in multipath MIMO systems.

Quadrature amplitude modulation (QAM) is widely used in modern communication systems, particularly mmWave systems. In this modulation, in-phase (I) and quadrature (Q) components should be perfectly matched. However, due to limited accuracy in practical systems, a perfect match is rarely possible, leading to performance degradation, including positioning. Although the effect of IQ imbalance (IQI) on positioning was studies previously in several papers (See for example [6]), to the best of our knowledge, it has not been investigated for 5G, despite its severity in mmWave systems [7]. IQI gain and phase parameters are usually compensated during the channel estimation phase [6], [8]. In mmWave systems, this is the phase during which DOD, DOA, and TOA are estimated and ultimately a position fix is obtained. This implies that investigating IQI jointly with localization is crucial in the context of 5G mmWave systems.

Fariba Ghaseminajm and Salama S. Ikki are with the Department of Electrical Engineering, Faculty of Engineering, Lakehead University, Thunder Bay, Ontario, Canada. Emails: {fghasemi, sikki}@lakeheadu.ca. Zohair Abu-Shaban and Craig R. Benson are with the School of Engineering and Information Technology, University of New South Wales (UNSW), Canberra, Australia. Emails: {zohair.abushaban, c.benson}@unsw.edu.au. Henk Wymeersch is with the Department of Signals and Systems, Chalmers University of Technology, Sweden. Email: henkw@chalmers.se.

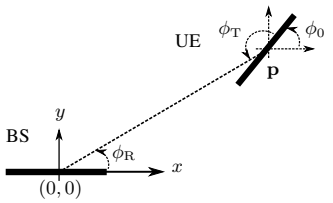

Fig. 1. Considered geometry including UE and BS equipped with of ULAs with N_{T} and N_{R} antennas respectively.

In this paper, we consider 2D mmWave uplink localization under IQI, focusing on the RF phase-shifting model [9]. To this end, we consider gain and phase imbalance at both the transmitter and receiver and derive the PEB and OEB. Subsequently, we investigate the resulting PEB and OEB degradation and obtain insights through numerical simulation.

II. Problem Formulation

Consider an uplink transmission scenario in which a BS is equipped with N_{R}-antenna uniform linear array (ULA) lying on the x-axis and centered at the origin. The BS receives a signal from a UE with an N_{T}-antenna ULA and an unknown orientation angle ϕ_0 measured from the positive x-axis, as shown in Fig. 1. We assume that the UE location, $\mathbf{p} = [p_x, p_y]^{\mathrm{T}}$, to be unknown. We assume one path between BS and UE as line of sight (LOS) channel. Note that in the case of multipath, the LOS provides the highest useful information in terms of positioning [4], and due to path orthogonality [2], it is easy to isolate it based on the received power profile.

A. Signal Model

The considered transceiver structure under I/Q mismatch is shown in Fig. 2. Based on [10] and [11], the baseband signal, $\mathbf{s}_{\mathrm{T}}(t) \triangleq [s_{\mathrm{T}_1}(t), \cdots, s_{\mathrm{T}_{N_{\mathrm{B}}}}(t)]^{\mathrm{T}}$, at the output of the RF chain can be written as

$$\mathbf{s}_{\mathrm{T}}(t) = \alpha_{\mathrm{T}}\mathbf{s}(t) + \beta_{\mathrm{T}}\mathbf{s}^*(t), \tag{1}$$

where $\mathbf{s}(t) \triangleq [s_1(t), \cdots, s_{N_{\mathrm{B}}}(t)]^{\mathrm{T}}$ is the baseband signal containing signals drawn from a zero-mean constellation and

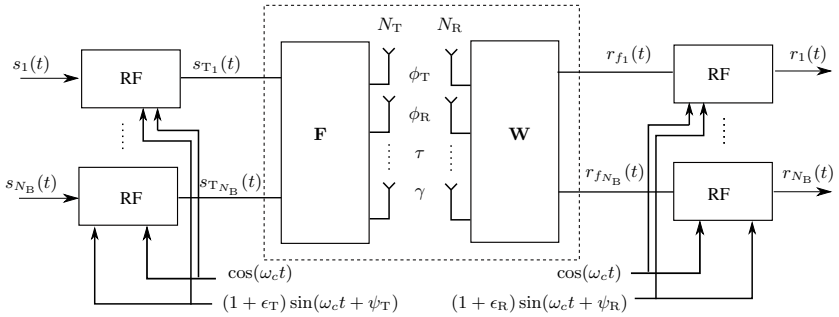

Fig. 2. 5G mmWave Transceiver structure under RF phase-shifting configuration ($\omega_c = 2\pi f_c$ where f_c is the carrier frequency)

passed through a pulse shaping filter with PSD $P(f)$, N_B is the number of transmitted beams and

$$\alpha_\mathrm{T} \triangleq \frac{1}{2}\left(1+m_\mathrm{T}e^{j\psi_\mathrm{T}}\right), \tag{2a}$$

$$\beta_\mathrm{T} \triangleq \frac{1}{2}\left(1-m_\mathrm{T}e^{j\psi_\mathrm{T}}\right), \tag{2b}$$

such that $m_\mathrm{T} \triangleq 1+\epsilon_\mathrm{T}$ and ϵ_T and ψ_T represent the amplitude and phase imbalance parameters of the transmitter outlined in Fig. 2. Note that E_s, the transmitted energy per symbol of $\mathbf{s}_\mathrm{T}(t)$, is related to E_t, the energy per symbol of $\mathbf{s}(t)$, by

$$E_\mathrm{s} = \frac{2E_\mathrm{t}}{1+m_\mathrm{T}^2}, \tag{3}$$

indicating that transmitter IQI leads to energy loss.

Denoting the DOD, DOA and propagation delay by $\phi_\mathrm{T}, \phi_\mathrm{R}$ and τ, respectively, a widely used model (e.g., [1], [2]) to describe the input/output relationship of the dashed box in Fig. 2 is

$$\begin{aligned}\mathbf{r}_\mathrm{f}(t) \triangleq &\sqrt{E_\mathrm{s}N_\mathrm{R}N_\mathrm{T}}\gamma\mathbf{W}^\mathrm{H}\mathbf{a}_\mathrm{R}(\phi_\mathrm{R})\mathbf{a}_\mathrm{T}{}^\mathrm{H}(\phi_\mathrm{T})\mathbf{F}\mathbf{s}_\mathrm{T}(t-\tau)\\ &+\mathbf{W}^\mathrm{H}\mathbf{n}(t), \in C^{N_\mathrm{B}},\end{aligned} \tag{4}$$

where $\gamma \triangleq \gamma_\mathrm{R}+j\gamma_\mathrm{I}$ is the complex path gain, and

$$\mathbf{a}_\mathrm{T}(\phi_\mathrm{T}) = \frac{1}{\sqrt{N_\mathrm{T}}}e^{-j\frac{2\pi d}{\lambda}\cos\phi_\mathrm{T}\mathbf{x}_\mathrm{T}}, \tag{5}$$

is the transmit array response vector, d is the inter-element spacing, and $\mathbf{x}_\mathrm{T} \triangleq \left[-\frac{N_\mathrm{T}-1}{2}, -\frac{N_\mathrm{T}-1}{2}+1, ..., \frac{N_\mathrm{T}-1}{2}\right]$ is the antenna location vector. $\mathbf{a}_\mathrm{R}(\phi_\mathrm{R})$ can be similarly defined. $\mathbf{F} = [\mathbf{f}_1, \cdots, \mathbf{f}_{N_\mathrm{B}}] \in \mathbb{C}^{N_\mathrm{T}\times N_\mathrm{B}}$ and $\mathbf{W} = [\mathbf{w}_1, \cdots, \mathbf{w}_{N_\mathrm{B}}] \in \mathbb{C}^{N_\mathrm{R}\times N_\mathrm{B}}$ are the N_B-beam analog transmit and receive beamforming matrices, respectively. Furthermore $\mathbf{n}(t) \triangleq [n_1(t), n_2(t), ..., n_{N_\mathrm{R}}(t)]^\mathrm{T} \in \mathbb{C}^{N_\mathrm{R}}$ denotes zero-mean additive white Gaussian noise with spectral density N_0, with independent real and imaginary parts.

Similar to the transmitter side, taking $m_\mathrm{R} \triangleq 1+\epsilon_\mathrm{R}$, then based on [10] and [11], the received baseband signal, $\mathbf{r}(t) \triangleq [r_1(t), \cdots, r_{N_\mathrm{B}}(t)]^\mathrm{T}$, is

$$\mathbf{r}(t) = \alpha_\mathrm{R}\mathbf{r}_\mathrm{f}(t) + \beta_\mathrm{R}\mathbf{r}_\mathrm{f}^*(t), \tag{6}$$

where the receiver IQI parameters are defined as

$$\alpha_\mathrm{R} \triangleq \frac{1}{2}\left(1+m_\mathrm{R}e^{-j\psi_\mathrm{R}}\right), \tag{7a}$$

$$\beta_\mathrm{R} \triangleq \frac{1}{2}\left(1-m_\mathrm{R}e^{j\psi_\mathrm{R}}\right). \tag{7b}$$

B. 2D localization problem

Our goal is to obtain the UE PEB and OEB using the received signal, $\mathbf{r}(t)$. We achieve this in two steps: first, we derive Fisher information of channel parameters $\boldsymbol{\varphi}_\mathrm{C} \triangleq \{\phi_\mathrm{R}, \phi_\mathrm{T}, \tau, \gamma_\mathrm{R}, \gamma_\mathrm{I}, \epsilon_\mathrm{R}, \epsilon_\mathrm{T}, \psi_\mathrm{R}, \psi_\mathrm{T}\}$. Then, we transfer this Fisher information into the position domain using a transformation of parameters.

III. FIM of Channel Parameters

We now derive the Fisher Information Matrix (FIM) of the vector of observed parameters. Namely, define

$$\boldsymbol{\varphi}_\mathrm{C} \triangleq [\phi_\mathrm{R}, \phi_\mathrm{T}, \tau, \gamma_\mathrm{R}, \gamma_\mathrm{I}, \epsilon_\mathrm{R}, \epsilon_\mathrm{T}, \psi_\mathrm{R}, \psi_\mathrm{T}]^\mathrm{T}, \tag{8}$$

then, the corresponding FIM is denoted by

$$\mathbf{J}_\mathrm{C} = \begin{bmatrix} J_{\phi_\mathrm{R}\phi_\mathrm{R}} & J_{\phi_\mathrm{R}\phi_\mathrm{T}} & \cdots & J_{\phi_\mathrm{R}\psi_\mathrm{T}} \\ J_{\phi_\mathrm{T}\phi_\mathrm{R}} & \ddots & \cdots & J_{\phi_\mathrm{T}\psi_\mathrm{T}} \\ \vdots & \vdots & \ddots & \vdots \\ J_{\psi_\mathrm{T}\phi_\mathrm{R}} & \cdots & \cdots & J_{\psi_\mathrm{T}\psi_\mathrm{T}} \end{bmatrix} \in \mathbb{R}^{9\times 9}. \tag{9}$$

The derivation of the elements in (9) depends on whether the noise covariance matrix is a function of the parameter in question [12]. Therefore, we digress to compute the noise covariance matrix as follows.

Taking $\mathbf{r}_\mathrm{o}(t-\tau) \triangleq \gamma\mathbf{W}^\mathrm{H}\mathbf{a}_\mathrm{R}(\phi_\mathrm{R})\mathbf{a}_\mathrm{T}{}^\mathrm{H}(\phi_\mathrm{T})\mathbf{F}\mathbf{s}_\mathrm{T}(t-\tau)$, based on (4) and (6), we can write

$$\begin{aligned}\mathbf{r}(t) = &\underbrace{\sqrt{E_\mathrm{s}N_\mathrm{R}N_\mathrm{T}}\left(\alpha_\mathrm{R}\mathbf{r}_\mathrm{o}(t-\tau)+\beta_\mathrm{R}\mathbf{r}_\mathrm{o}^*(t-\tau)\right)}_{\boldsymbol{\mu}(t)}\\ &+\underbrace{\left(\alpha_\mathrm{R}\mathbf{W}^\mathrm{H}\mathbf{n}(t)+\beta_\mathrm{R}\mathbf{W}^\mathrm{T}\mathbf{n}^*(t)\right)}_{\mathbf{z}(t)}.\end{aligned} \tag{10}$$

In order to simplify the exposition, we assume orthogonal beams such that $\mathbf{W}^\mathrm{H}\mathbf{W} = \sigma_b^2\mathbf{I}_{N_\mathrm{B}}$, in which σ_b^2 is the power per beam. This is a reasonable assumption due to the sparse transmission in 5G mmWave channels [1]. Consequently, the noise variance can be written as

$$\boldsymbol{\Sigma}_z = \mathbb{E}\left[\mathbf{z}(t)\mathbf{z}^\mathrm{H}(t)\right] = N_0\sigma_b^2\left(|\alpha_\mathrm{R}|^2+|\beta_\mathrm{R}|^2\right)\mathbf{I}_{N_\mathrm{B}} \tag{11a}$$

$$= \underbrace{\frac{1}{2}N_0(1+m_\mathrm{R}^2)\sigma_b^2}_{\triangleq\sigma_z^2}\mathbf{I}_{N_\mathrm{B}}. \tag{11b}$$

where (11a) follows from the fact that $\mathbb{E}\left[\mathbf{n}(t)\mathbf{n}^\mathrm{T}(t)\right] = \mathbf{0}$, and (11b) follows from (7). Note that as ϵ_R increases linearly, the noise covariance at the receiver increases quadratically.

From (11), it is clear that the only parameter in $\boldsymbol{\varphi}_{\mathrm{C}}$ that σ_z^2 depends on is ϵ_{R}. Thus, from [12], it can be shown that

$$J_{\epsilon_{\mathrm{R}}\epsilon_{\mathrm{R}}} = \frac{1}{\sigma_z^2}\int_0^{T_0} \mathbb{E}\left\|\frac{\partial \boldsymbol{\mu}(t)}{\partial \epsilon_{\mathrm{R}}}\right\|^2 \mathrm{d}t + \frac{T_0 N_{\mathrm{B}}^2}{2(\sigma_z^2)^2}\left(\frac{\partial {\sigma_z}^2}{\partial \epsilon_{\mathrm{R}}}\right)^2 \quad (12)$$

while for all the other parameters in $\boldsymbol{\varphi}_{\mathrm{C}}$, we have

$$\begin{aligned} J_{xy} &\triangleq \int_0^{T_0} \mathbb{E}\left[\Re\left\{\frac{\partial \boldsymbol{\mu}^{\mathrm{H}}(t)}{\partial x}\left(\boldsymbol{\Sigma}_{\boldsymbol{Z}}\right)^{-1}\frac{\partial \boldsymbol{\mu}(t)}{\partial y}\right\}\right]\mathrm{d}t, \\ &= \frac{1}{\sigma_z^2}\int_0^{T_0} \mathbb{E}\left[\Re\left\{\frac{\partial \boldsymbol{\mu}^{\mathrm{H}}(t)}{\partial x}\frac{\partial \boldsymbol{\mu}(t)}{\partial y}\right\}\right]\mathrm{d}t, \end{aligned} \quad (13)$$

where $x, y \in \{\phi_{\mathrm{R}}, \phi_{\mathrm{T}}, \tau, \gamma_{\mathrm{R}}, \gamma_{\mathrm{I}}, \epsilon_{\mathrm{T}}, \psi_{\mathrm{R}}, \psi_{\mathrm{T}}\}$, $T_0 \approx N_{\mathrm{s}} T_{\mathrm{s}}$ is the observation time and N_{s} is the number of pilot symbols. The full derivation of the elements of (9) is tedious but straight forward, so it is provided in [13].

The parameters in $\boldsymbol{\varphi}_{\mathrm{C}}$ can be divided into two groups: geometrical parameters providing information useful for positioning, and nuisance parameters. We are mainly interested in the equivalent FIM [2] of the geometrical parameters that accounts for the nuisance parameters. Towards that, defining the vector of geometrical parameters as $\boldsymbol{\varphi}_{\mathrm{G}} \triangleq [\phi_{\mathrm{R}}, \phi_{\mathrm{T}}, \tau]^{\mathrm{T}}$, and the vector of nuisance parameters as $\boldsymbol{\varphi}_{\mathrm{N}} \triangleq [\gamma_{\mathrm{R}}, \gamma_{\mathrm{I}}, \epsilon_{\mathrm{R}}, \epsilon_{\mathrm{T}}, \psi_{\mathrm{R}}, \psi_{\mathrm{T}}]^{\mathrm{T}}$, we can write (9) in block form as

$$\mathbf{J}_{\mathrm{C}} = \begin{bmatrix} \mathbf{J}_{\mathrm{G}} & \mathbf{J}_{\mathrm{GN}} \\ \mathbf{J}_{\mathrm{GN}}^{\mathrm{T}} & \mathbf{J}_{\mathrm{N}} \end{bmatrix} \in \mathbb{R}^{9\times 9}, \quad (14)$$

where $\mathbf{J}_{\mathrm{G}} \in \mathbb{R}^{3\times 3}$ and $\mathbf{J}_{\mathrm{N}} \in \mathbb{R}^{6\times 6}$ are the FIMs of $\boldsymbol{\varphi}_{\mathrm{G}}$ and $\boldsymbol{\varphi}_{\mathrm{N}}$, respectively, while $\mathbf{J}_{\mathrm{GN}}$ is the mutual information matrix of $\boldsymbol{\varphi}_{\mathrm{G}}$ and $\boldsymbol{\varphi}_{\mathrm{N}}$. Consequently, the EFIM of $\boldsymbol{\varphi}_{\mathrm{G}}$ is computed using Schur complement as [14]

$$\mathbf{J}_{\mathrm{G}}^{\mathrm{e}} = \mathbf{J}_{\mathrm{G}} - \mathbf{J}_{\mathrm{GN}}\mathbf{J}_{\mathrm{N}}^{-1}\mathbf{J}_{\mathrm{GN}}^{\mathrm{T}}. \quad (15)$$

Note that the minus sign in (15) indicates loss of information due to the nuisance parameters.

IV. FIM of Location Parameters

As highlighted earlier, our goal is to derive the PEB and OEB from the intermediary parameters, i.e., channel parameter. To this end, the FIM of position and orientation, $\boldsymbol{\varphi}_{\mathrm{L}} \triangleq [p_x, p_y, \phi_0]^{\mathrm{T}}$, can be computed via a transformation of parameters as follows [12]

$$\mathbf{J}_{\mathrm{L}}^{\mathrm{e}} \triangleq \boldsymbol{\Upsilon}\mathbf{J}_{\mathrm{G}}^{\mathrm{e}}\boldsymbol{\Upsilon}^{\mathrm{T}}, \quad (16)$$

where $\boldsymbol{\Upsilon}$ is the transformation matrix, given by the Jacobean

$$\boldsymbol{\Upsilon} = \frac{\partial \boldsymbol{\varphi}_{\mathrm{G}}^{\mathrm{T}}}{\partial \boldsymbol{\varphi}_{\mathrm{L}}} = \begin{bmatrix} \frac{\partial \phi_{\mathrm{R}}}{\partial p_{\mathrm{x}}} & \frac{\partial \phi_{\mathrm{T}}}{\partial p_{\mathrm{x}}} & \frac{\partial \tau}{\partial p_{\mathrm{x}}} \\ \frac{\partial \phi_{\mathrm{R}}}{\partial p_{\mathrm{y}}} & \frac{\partial \phi_{\mathrm{T}}}{\partial p_{\mathrm{y}}} & \frac{\partial \tau}{\partial p_{\mathrm{y}}} \\ \frac{\partial \phi_{\mathrm{R}}}{\partial \phi_0} & \frac{\partial \phi_{\mathrm{T}}}{\partial \phi_0} & \frac{\partial \tau}{\partial \phi_0} \end{bmatrix} \in \mathbb{R}^{3\times 3}. \quad (17)$$

The entries of $\boldsymbol{\Upsilon}$ can be obtained from the relationships between the UE and BS highlighted in the geometry shown in Fig. 1. That is, defining c as the propagation speed

$$\tau = \frac{\|\mathbf{p}\|}{c}, \quad (18a)$$

$$\phi_{\mathrm{R}} = \arccos\left(\frac{p_x}{\|\mathbf{p}\|}\right), \quad (18b)$$

$$\phi_{\mathrm{T}} = \pi - \phi_0 + \arccos\left(\frac{p_x}{\|\mathbf{p}\|}\right). \quad (18c)$$

Finally, for brevity, define $\mathbf{C} = (\mathbf{J}_{\mathrm{G}}^{\mathrm{e}})^{-1}$, then the PEB and OEB under IQI can be found as

$$\mathrm{PEB}_{\mathrm{IQ}} = \sqrt{[C]_{1,1} + [C]_{2,2}}, \quad (19a)$$

$$\mathrm{OEB}_{\mathrm{IQ}} = \sqrt{[C]_{3,3}}. \quad (19b)$$

V. Numerical results

A. Simulation Setup

We consider a mmWave scenario operating at $f = 38$ GHz. The BS is equipped with $N_{\mathrm{R}} = 64$ antennas and located at $(0, 0)$. On the other hand, the UE is located in a square area, (10 m×10 m), defined by $(p_x, p_y) \in \{(x, y) : y \geq |x| \cap y \leq 10\sqrt{2} - |x|\}$ and equipped with $N_{\mathrm{T}} = 32$ antennas.

We utilize directional beamforming similar to [2], in which beams point toward $\phi_{B,l}, 1 \leq l \leq N_{\mathrm{B}}$, such that the transmit and receive beamforming are respectively given by

$$\mathbf{f}_l \triangleq \frac{1}{\sqrt{N_{\mathrm{B}}}}\mathbf{a}_{\mathrm{T}}(\phi_{BT,l}),$$
$$\mathbf{w}_l \triangleq \frac{1}{\sqrt{N_{\mathrm{B}}}}\mathbf{a}_{\mathrm{R}}(\phi_{BR,l}),$$

where $\mathbf{a}_{\mathrm{T}}(\phi_{BT,l})$ and $\mathbf{a}_{\mathrm{R}}(\phi_{BR,l})$ have the same structure as (5). We chose $N_{\mathrm{B}} = 18$, uniformly covering the square area, i.e., $\phi_{BR,l} = \frac{\pi}{4} + \frac{\pi(l-1)}{2(N_{\mathrm{B}}-1)}$.

Furthermore, we assume $\mathbf{s}_{\mathrm{T}}(t)$ to be transmitted through a unit energy ideal $sinc$ pulse shaping filter so that the effective bandwidth, $W_{\text{eff}}^2 = W^2/3$ where $W = 125$ MHz. Moreover we use the following parameters $N_0 = -170$ dBm/Hz, $N_{\mathrm{s}} = 16$, $\sigma_b^2 = 1$ and $\phi_0 = 0$. We conduct Monte-Carlo simulations for 120 UE locations and average over 100 iterations to obtain the PEB and OEB degradation due to IQI

$$\mathrm{PEB}_{\text{deg}} = \frac{\mathrm{PEB}_{\mathrm{IQ}} - \mathrm{PEB}_{\text{match}}}{\mathrm{PEB}_{\text{match}}} \times 100\%,$$
$$\mathrm{OEB}_{\text{deg}} = \frac{\mathrm{OEB}_{\mathrm{IQ}} - \mathrm{OEB}_{\text{match}}}{\mathrm{OEB}_{\text{match}}} \times 100\%$$

where $\mathrm{PEB}_{\text{match}}$ and $\mathrm{OEB}_{\text{match}}$ are defined similar to (19) after dropping $\epsilon_{\mathrm{R}}, \epsilon_{\mathrm{T}}, \psi_{\mathrm{R}}$ and ψ_{T} from $\boldsymbol{\varphi}_{\mathrm{N}}$ and setting them to zero in (1) and (6) .

B. PEB and OEB with respect to I/Q parameters

Fig. 3 shows user PEB percentage degradation with respect to transmitter I/Q parameters for the considered scenario. For this figure, the receiver parameters are chosen randomly over the ranges $-0.5 \leq \epsilon_{\mathrm{R}} \leq 0.5$ and $-30^\circ \leq \psi_{\mathrm{R}} \leq 30^\circ$. It can be seen that minimum degradation occurs when $\epsilon_{\mathrm{T}} = \psi_{\mathrm{T}} = 0$. That is, transmitter I and Q branches are perfectly matched. Moreover, the PEB percentage degradation increases gradually as the imbalance deteriorates by diverging from the point $\epsilon_{\mathrm{T}} = \psi_{\mathrm{T}} = 0$. It worth noting that the general behavior of PEB percentage degradation is almost symmetrical along ψ_{T}, unlike ϵ_{T}. To see this clearer, we present Fig. 4. It is intuitive that as ϵ_{T} increases, the IQI worsens and its impact on PEB degradation increases. However, it can be seen that as

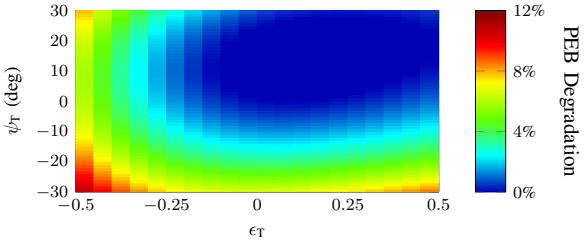

Fig. 3. PEB degradation with respect to ϵ_{T} and ψ_{T}. $N_{\mathrm{T}} = 32$, $N_{\mathrm{R}} = 64$, $N_{\mathrm{B}} = 18$ and $\phi_0 = 0$

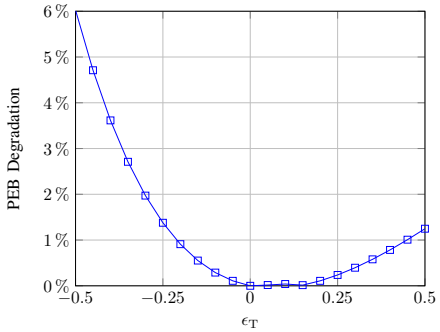

Fig. 4. PEB degradation at $\psi_{\mathrm{T}} = 0$.

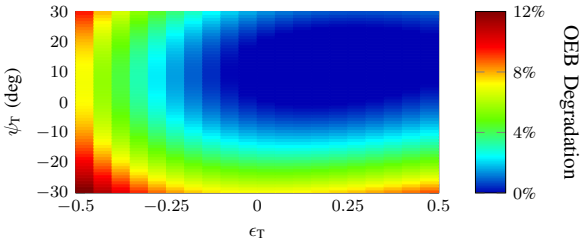

Fig. 5. OEB degradation with respect to ϵ_{T} and ψ_{T}. $N_{\mathrm{T}} = 32$, $N_{\mathrm{R}} = 64$, $N_{\mathrm{B}} = 18$ and $\phi_0 = 0$

ϵ_{T} decreases towards negative values, the degradation becomes more pronounced. This occurs because the magnitude of the quadrature carrier signal diminishes, i.e., $m_{\mathrm{T}} \sin(\omega_c t + \psi_{\mathrm{T}})$ and both $\mathrm{PEB}_{\mathrm{IQ}}$ and $\mathrm{PEB}_{\mathrm{match}}$ worsen. Considering a system-level evaluation, it can be seen that for relevant values of ϵ_{T} and ψ_{T}, there is up to 15% bound degradation due to IQI.

Fig. 5 presents the OEB percentage degradation with respect to the transmitter I/Q parameters. In general, the behavior of OEB degradation is similar to that of the PEB degradation although around the corners OEB is slightly higher. In [2], it has been shown that PEB is a function of DOD and TOA, while OEB is a function of DOA and DOD. Therefore the slight deterioration of OEB with respect to PEB is due the additional in estimating DOA, arising from IQI.

As shown in Fig. 6, the PEB percentage degradation with respect to the receiver I/Q parameters exhibits a similar behavior to that with respect to the transmitter parameter, except that contour plots are flipped w.r.t $\psi_{\mathrm{R}} = 0$. This is due to the different signs in (2a) and (7a). Moreover, a similar observation can be made on the behavior of OEB with respect to the receiver parameters [13].

VI. Conclusion

In this paper, we investigated the effects of I/Q imbalance phenomenon on the position and orientation error bounds.

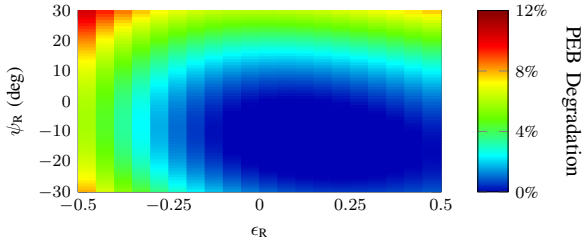

Fig. 6. PEB degradation with respect to ϵ_{R} and ψ_{R}. $N_{\mathrm{T}} = 32$, $N_{\mathrm{R}} = 64$, $N_{\mathrm{B}} = 18$ and $\phi_0 = 0$

We considered 2D 5G mmWave uplink localization with analog beamforming. Our results show that PEB and OEB degrade by similar amounts with respect to amplitude and phase imbalance. While this degradation is symmetric with respect to the phase imbalance, it is more significant for negative amplitude errors than positive. We also showed that I/Q imbalance can cause up to 12% increase in the error of location and orientation estimation. For future work, we will consider different transceiver structures such as IF phase-shifting, LO phase shifting and hybrid beamforming.

References

[1] R. W. Heath, N. Gonzlez-Prelcic, S. Rangan, W. Roh, and A. M. Sayeed, "An overview of signal processing techniques for millimeter wave MIMO systems," *IEEE Journal of Selected Topics in Signal Processing*, vol. 10, no. 3, pp. 436–453, April 2016.

[2] Z. Abu-Shaban, X. Zhou, T. Abhayapala, G. Seco-Granados, and H. Wymeersch, "Error bounds for uplink and downlink 3D localization in 5G millimeter wave systems," *IEEE Transactions on Wireless Communications*, vol. 17, no. 8, pp. 4939–4954, Aug 2018.

[3] A. Shahmansoori, G. E. Garcia, G. Destino, G. Seco-Granados, and H. Wymeersch, "Position and orientation estimation through millimeter-wave MIMO in 5G systems," *IEEE Transactions on Wireless Communications*, vol. 17, no. 3, pp. 1822–1835, March 2018.

[4] C. E. O'Lone, H. S. Dhillon, and R. M. Buehrer, "Single-anchor localizability in 5G millimeter wave networks," *IEEE Wireless Communications Letters*, pp. 1–1, Sep. 2019.

[5] Y. Wang, Y. Wu, and Y. Shen, "Joint spatiotemporal multipath mitigation in large-scale array localization," *IEEE Transactions on Signal Processing*, vol. 67, no. 3, pp. 783–797, Feb 2019.

[6] T. Nguyen, J. Louveaux, P. De Doncker and F. Horlin, "Impact of I/Q Imbalance on Time Reversal-based Indoor Positioning Systems," 2018 14th International Conference on Wireless and Mobile Computing, Networking and Communications (WiMob), Limassol, 2018, pp. 36-41.

[7] X. Yang, M. Matthaiou, J. Yang, C. Wen, F. Gao, and S. Jin, "Hardware-constrained millimeter-wave systems for 5G: Challenges, opportunities, and solutions," *IEEE Communications Magazine*, vol. 57, no. 1, pp. 44–50, January 2019.

[8] M. Aziz, F. M. Ghannouchi, M. Helaoui. "Blind Compensation of I/Q Impairments in Wireless Transceivers," *Sensors*, vol. 17, no. 12, Dec 2017.

[9] M. Fakharzadeh, M. Nezhad-Ahmadi, B. Biglarbegian, J. Ahmadi-Shokouh, and S. Safavi-Naeini, "CMOS phased array transceiver technology for 60 GHz wireless applications," *IEEE Transactions on Antennas and Propagation*, vol. 58, no. 4, pp. 1093–1104, April 2010.

[10] T. Schenk, *RF Imperfections in High-rate Wireless Systems: Impact and Digital Compensation*. Springer Netherlands, 2008.

[11] R. Mesleh, S. S. Ikki, and F. S. Almehmadi, "Impact of I/Q imbalance on the performance of qsm multiple-inputmultiple-output system," *IET Communications*, vol. 10, no. 17, pp. 2391–2395, 2016.

[12] S. M. Kay, *Fundamentals of Statistical Signal Processing: Estimation Theory*. NJ, USA: Prentice-Hall, Inc., 1993.

[13] F. Ghaseminajm, Z. Abu-Shaban, S. S. Ikki, H. Wymeersch, and C. R. Benson, "Localization error bounds for 5G mmwave systems under I/Q imbalance: An extended version," *arXiv*, Nov. 2019. [Online]. Available: https://arxiv.org/abs/1911.06124.

[14] Y. Shen and M. Z. Win, "Fundamental limits of wideband localization – part I: A general framework," *IEEE Trans. on Inf. Theory*, vol. 56, no. 10, pp. 4956–4980, Oct 2010.